COBEM 99
XV Congresso Brasileiro de Engenharia Mecânica
15th Brazilian Congress of Mechanical Engineering
22 - 26 de Novembro de 1999 / November 22 - 26, 1999 Águas de Lindóia, São Paulo,

Three-dimensional Supersonic Flow Over a Spike-Nosed Body of Revolution

ALGACYR MORGENSTERN JR.
Divisão de Sistemas Espaciais - CTA/Instituto de Aeronáutica e Espaço
CEP 12228-904 São José dos Campos, SP, Brasil - E-mail: algacyr@ase-n2.iae.cta.br

Abstract

The unsteady, viscous, supersonic flow over a spike-nosed body of revolution was numerically investigated by solving the Navier-Stokes equations. The time-accurate computations were performed employing an implicit algorithm based on the second-order time accurate LU-SGS scheme with the incorporation of a subiteration procedure to maintain time accuracy. The characteristics of the flow field for a Mach number of 3.0, Reynolds number of 7.87 x 10^6/m, and angles of attack of 5 and 10 degrees are described. Self-sustained asymmetric shock wave oscillations were observed in the numerical computations for these angles of attack. The main characteristics of the flow field, as well as its influence on drag coefficient is discussed.

Keywords: unsteady flow; supersonic flow; spike-nosed body; time-accurate computations; Newton-like subiterations.

1. INTRODUCTION

Spikes ahead of the blunt noses of bodies of revolution have been investigated as a means of drag reduction and heat flux attenuation by a number of investigators. Crawford (1959) experimentally investigated the effects of spike-nosed blunt bodies on heat flux and pressure drag for a Mach number of 6.8 and a wide range of Reynolds numbers. In this work it was assessed the effects of varying spike length on pressure drag and heat transfer, which indicated the strong influence of Reynolds number on heat transfer and spike length on drag reduction. The experimental investigations of Bogdonoff and Irwin (1959) indicated that the shock-wave configuration in front of spike-tipped axisymmetric bodies in high-speed flows could be unstable. This instability arises primarily in cases where the forebody geometry has a forward-facing step. Later on, Demetriades and Hopkins (1977) conducted experiments at supersonic speeds for an axisymmetric spike geometry. In this work it was reported observations which implied a more complex shock motion than that previously imagined; the shock motion was thought limited to one degree of freedom in the radial direction; shock expanding-collapsing symmetrically about the body axis. It was suggested that one more degree of freedom exist. The shock oscillations would rotate about the spike. A more recent experimental investigation performed by Calarese and Hankey (1985) revealed the unstable shock structure as consisting of a strong detached bow shock at the spike's tip which then collapses into a conical shock that intersects a quasi normal shock near the body's shoulder. It was also given evidence that

the shock oscillates axially in a symmetric fashion with respect to the spike as well as in an asymmetric fashion for certain configurations and flow conditions. This phenomenon is highly unstable, and the necessary conditions for it to occur are the presence of a shear layer with an inflection point in the velocity profile, a reflecting surface, and the appropriate spike length to permit in phase reflections of pressure waves. If these conditions are met, highly organized oscillations of the impinging flow are sustained by feedback of upstream pressure propagation through the subsonic separated region to the shear layer origin, and by amplification of the disturbances until a limit cycle is reached.

Numerical solutions for flows over spike-nosed bodies can be found as late as the beginning of last decade. Shang, et. al. (1980), investigated the longitudinal mode of oscillations, the pressure amplitude of the disturbance as well as the shear layer and shock wave systems. Shoemaker (1990) performed a numerical investigation of an optimal spike-nosed configuration to minimize drag at a design Mach number of 2.5. Mikhail (1991 and 1996) investigated the flow over projectiles with a spike-nosed configuration and tripping rings.

In all of these investigations, however, the flow around spike-nosed bodies were studied only for zero angle of attack. More recently, Yamauchi, et. al., (1995) computed numerically the flow around a spiked blunt body for angles of attack larger than zero. The geometry considered in these studies resulted in steady flows. Although these efforts succeeded in simulate this complex flow, the characteristics of the unsteady flow for angles of attack larger than zero has not been discussed.

In the present paper, supersonic flows over a spike-nosed body are numerically simulated to study the effects of varying angle of attack for an originally unsteady flow field at zero angle of attack. It is not assumed any symmetry of the flow field in order to capture any disturbance in the radial as well as axial directions.

2. PROBLEM DEFINITION AND SOLUTION APPROACH

2.1 Body Geometry

The geometry of the configuration used in the present study is shown in Fig. 1. It was used the same spike-nosed body configuration that Calarese and Hankey (1985) employed in their experiments. The model is an axisymmetric cone frustum with a 9° cone angle.

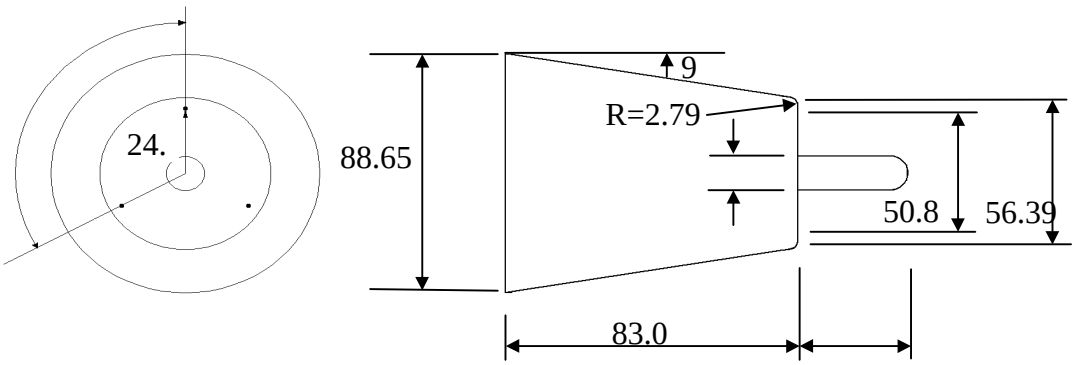

Figure 1. Geometry of the configuration. Dimensions in mm.

2.2 Flow Conditions

Freestream Mach number is 3.0, Reynolds is 7.87 x 10^6/m, and the flow is assumed to be laminar. This assumption was made since the characteristic length scales are limited to 38.1 mm. The Reynolds number based on the running length is 2.998 x 10^5 which ensures that the flow is initially laminar. The flow conditions were selected for comparison with experimental data in axisymmetric flows. Although, for this geometry and flow conditions Calarese and Hankey (1985) did not report asymmetries for zero angles of attack, in this numerical investigation a full three-dimensional flow was considered to allow any asymmetry to develop in the cases of angles of attack larger than zero.

2.3 Computational Grid

The three-dimensional computational grid employed in this study is presented in Figure 2. The number of grid points in the axial, circumferencial, and radial, directions are 121x37x81 respectively. The grid was constructed by rotating a 121x81 two-dimensional grid in 10 degrees intervals.

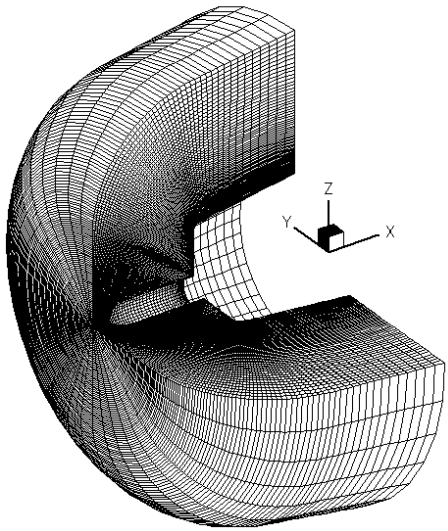

Figure 2. Computational grid, 121x37x81 grid points

2.4 Numerical Algorithm

The compressible laminar flow over a spike-nosed body is governed by the Navier-Stokes equations, which are written in strong conservation law form in a generalized coordinate system. The equations are solved using the lower-upper symmetric-Gauss-Seidel factorization scheme proposed by Yoon, S. and Kwak, D. (1992). The advantage of this factorization scheme is that the construction of the diagonal of the L and U matrices permits a scalar inversion, leading to a very efficient and vectorizable algorithm. To ensure time accuracy a Newton-like sub-iteration procedure presented in Matsuno (1989) is introduced.

2.5 Initial and Boundary Conditions

The initial flowfield is set to be freestream everywhere. All variables are extrapolated at the outflow boundary and nonslip wall condition is applied on the surface of the body. Isothermal wall condition is imposed with wall temperature of 311 K.

3. RESULTS AND DISCUSSION

3.1 Axisymmetric Flow

The fully three-dimensional axisymmetric flow at zero angle of attack was computed to compare the results with data obtained by the experimental investigation of Calarese and Hankey (1985), and numerically computed results of Morgenstern (1997). The latter were obtained employing an axisymmetric formulation. Fig. 3 shows the comparison of the spectral estimate of a pressure time history data sample collected at a radius of 24.13 mm on the frustum face as indicated in figure 1. The primary mode associated with axial shock oscillations has a fundamental frequency of about 2800 Hz. The computed results captured all nine frequencies with very good accuracy when compared with the experiments. The experimental observation of an oscillation wave being modulated with another wave of about half the frequency was also present in the computed results. The comparison between the numerical results also show good agreement, confirming the experimental evidence that for this geometry and flow condition the flow is axisymmetric.

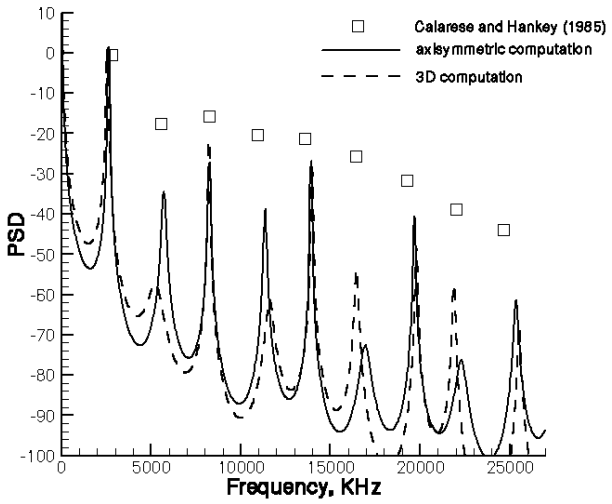

Figure 3. Power spectral estimate. Axisymmetric

3.2 Effects of Angle of Attack

The main characteristics of the flow over a spike-nosed body at an angle of attack larger than zero is described in Figures 4a-4c. Velocity vectors and density contour plots are shown for an instant in time at $\alpha = 10°$ in three streamwise planes corresponding to $\theta = 0$, 90, and

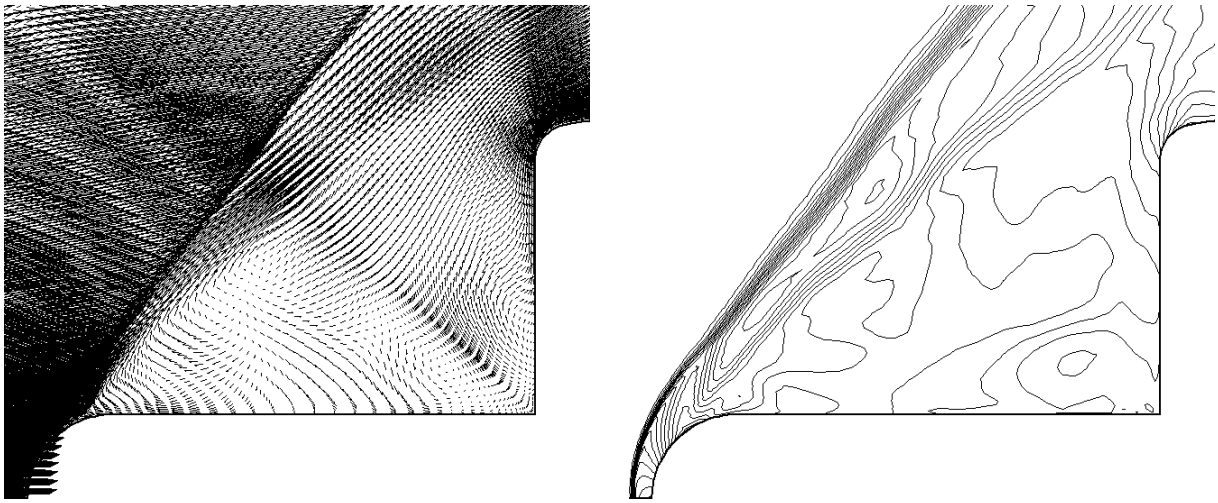

a) Velocity vector and density contour plots on the $\theta = 0°$ plane.

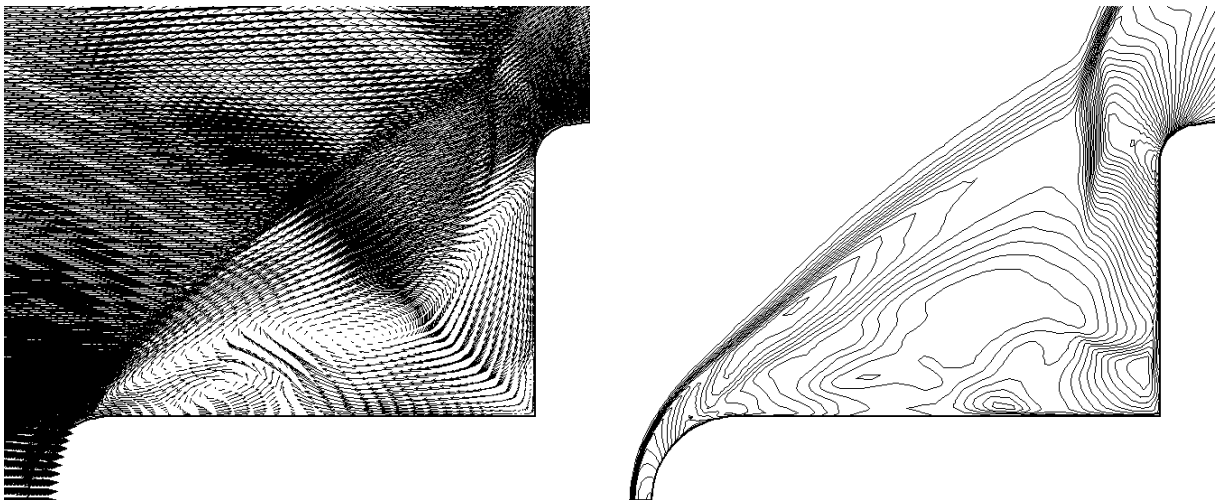

b) Velocity vector and density contour plots on the $\theta = 90°$ plane.

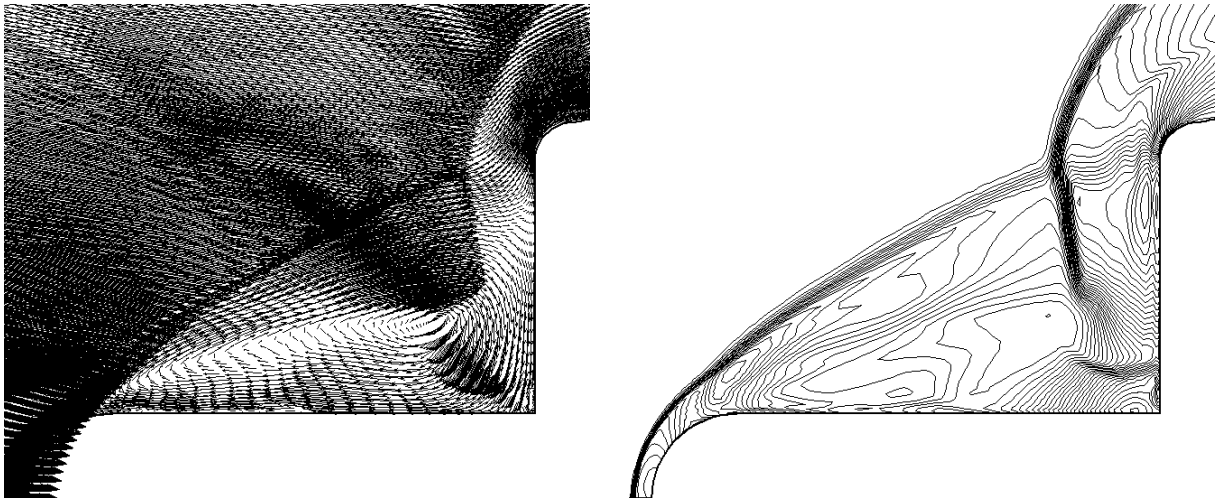

c) Velocity vector and density contour plots on the $\theta = 180°$ plane.

Figure 4. Instantaneous flowfield for $\alpha = 10°$.

180 degrees, respectively. In Fig. 4a, corresponding to the leeward side, $\theta = 0°$, the oblique bow shock wave from the nose of the spike interacts with the reattachment shock wave from the frustum corner above the body. At this instant in time the shear layer pass over the frustum face providing a relieve in pressure within the separated region over the spike. A large separated region is observed in front of the frustum. Fig. 4b shows the lateral position, corresponding to $\theta = 90°$. At this position the conical bow shock wave interacts with a quasi-normal reflected shock wave from the frustum face. This quasi-normal shock wave is originated due to the collapse of the separated shear layer into the frustum face at the reattachment point, which then pumps high pressure flow upstream. The reattachment point of the separated shear layer occurs close to the frustum corner. The separated region over the spike displays a more complex flow structure with secondary separations, vortical structures,

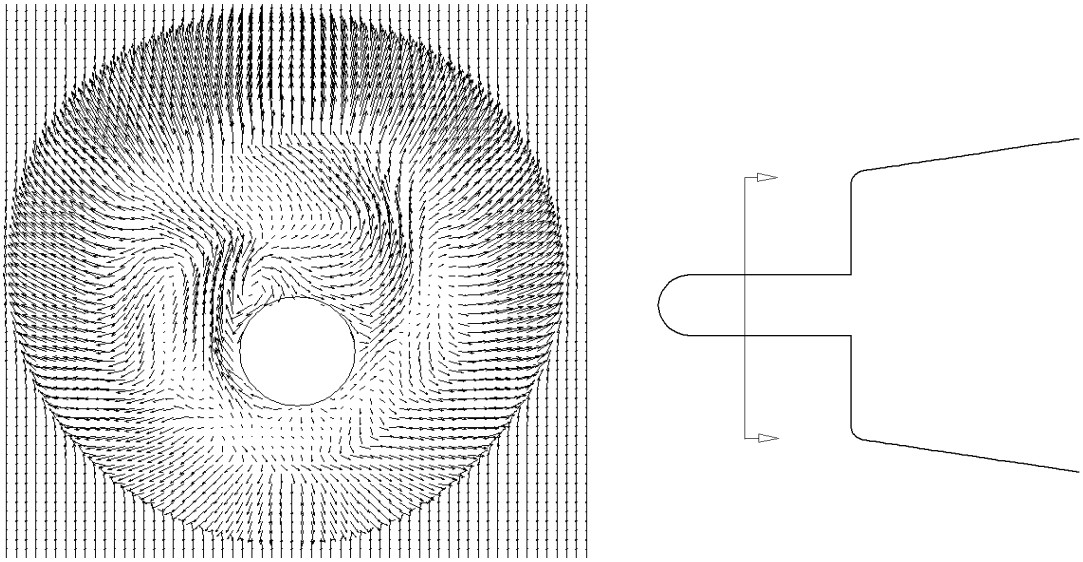

Figure 5. Cross flow velocity Vectors

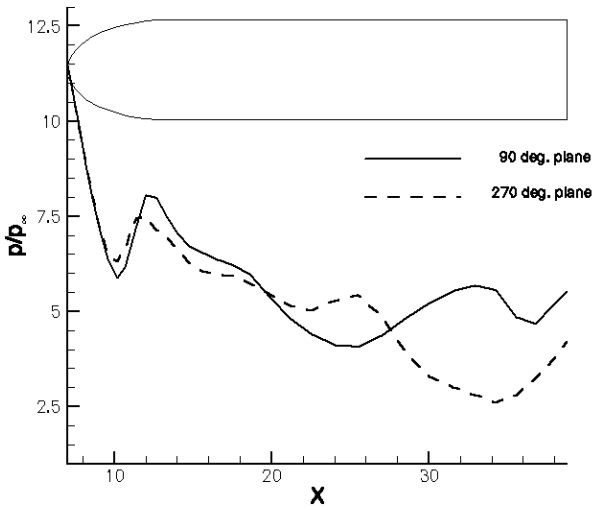

Figure 6. Instantaneous Pressure Distribution, $\alpha=10°$.

and shock waves. Fig. 4c shows the windward position, corresponding to $\theta = 180°$. The same flow structure found for the $\theta = 90°$ plane can be observed. The shear layer impinges on the frustum face at a steeper angle resulting in stronger reflected shock waves. The cross flow over the spike can be seen in Fig. 5. Velocity vectors around the spike present an asymmetric vortex shedding pattern. This vortex shedding, originated at the secondary separation on the spike, causes a sudden burst of pressure in one side of the spike, being responsible for asymmetric disturbances on the shock structure. Fig. 6 shows the instantaneous pressure distribution on the 90 and 270 degrees planes, illustrating this asymmetry.

3.2 Unsteadiness of the Flow

The flow over the spike-nosed body at 5 degrees angle of attack is described by a sequence of instantaneous plots shown in Figs. 7 over one cycle of shock oscillation. Figures 7a show the flowfield velocity vectors and density contours on the spike surface, and 7b show flowfield and spike surface density contours. At time t_1 the shock structure starts to move upstream driven by a reflected shock wave from the frustum face. It continues its movement upstream in time t_2 until the shear layer escapes from the frustum face edge. This causes a pressure relieving effect that trigger the downstream motion of the shock structure, time t_3, that continues through time t_4, until the shock structure interacts again with the frustum face, closing the cycle. This cycle is repeated in a periodic fashion.

For zero angle of attack this oscillation cycle occurs in an axisymmetric fashion. For angles of attack different from zero the flow in the leeward and windward positions display a non-symmetric character as can be seen in figures 7a and 7b. Moreover, as observed in the previous section, Fig. 6, an oscillation wave in the lateral direction is generated by the asymmetric pressure distribution on the sides of the spike. The integrated forces in the axial, *x*, lateral, *y*, and normal, *z*, directions over one cycle of oscillations are shown in Figure 8. The oscillatory behavior of the flow field can be clearly observed. It is also shown that although the magnitude of the force increase with increasing angle of attack, the amplitude of the oscillations decreases with increasing angle of attack. The lateral force coefficient, *cfy*, also shows oscillations, however at a much smaller amplitude.

Power spectral estimate of the pressure time history at the leeward and windward positions on the frustum face for the $\alpha = 5°$ flow is shown in figure 9. In the windward plane all nine modes of oscillations found in the axisymmetric case are present. However, in the leeward plane only the first mode, the primary mode associated with the axial shock oscillations, is in agreement. The other modes of oscillation are shifted or not present. This is attributed to the vortex shedding from the sides of the spike that interfere with the shock oscillations on the leeward side of the spike.

3.3 Drag Coefficient

Drag coefficients for the angles of attack considered were computed from the averaged flow fields. These computations include both pressure and viscous contributions. However, the contribution from the base region is not included, i.e., the pressure in the base region is assumed to have the freestream value when computing the drag coefficient. As seen in Table 1 the drag coefficient increases with increasing angle of attack. However it is worth noting that from zero to 5 degrees angle of attack the drag coefficient increased 8% and from 5 to 10 degrees it increased 3.7%. This reduction in the increase of the drag coefficient with

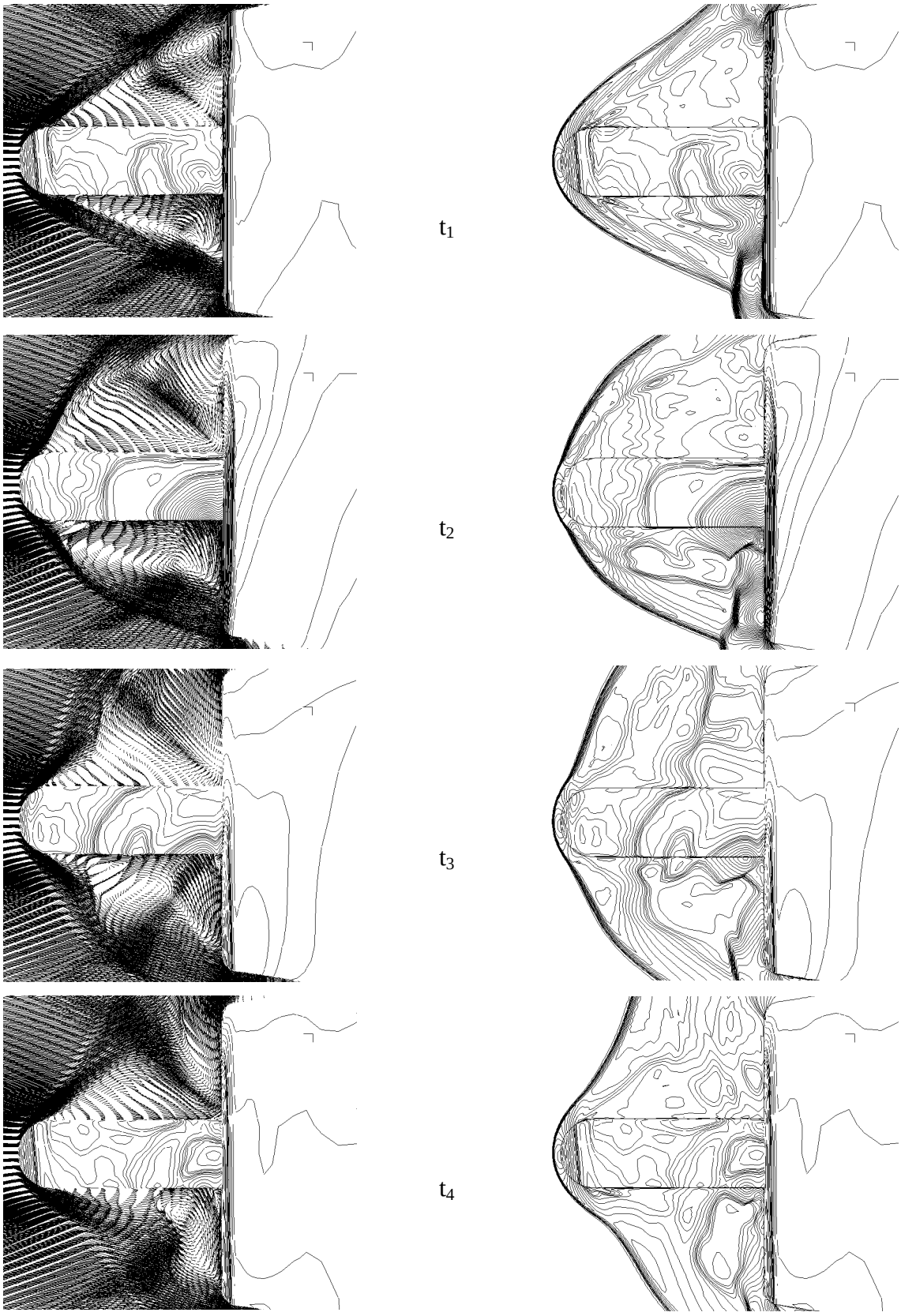

a) Velocity Vectors b) Density contours

Figure 7. Shock wave oscillations, one cycle, $\Delta t = 70.99\ \mu s$, $\alpha = 5°$.

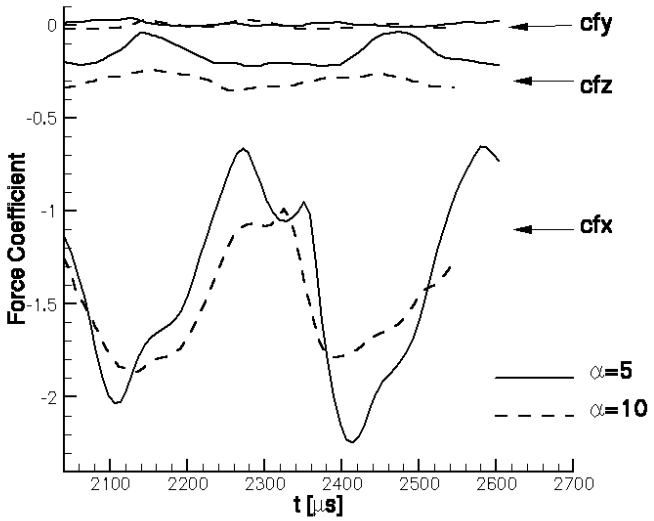

Figure 8. Time history of the integrated forces

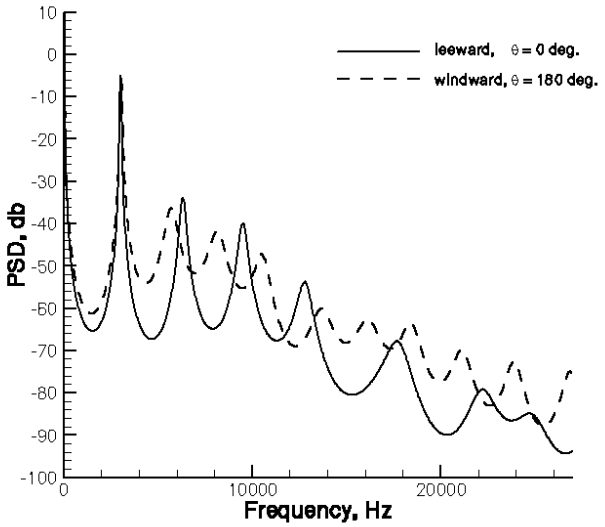

Figure 9. Power spectral estimate. $\alpha = 5°$ flow.

increasing angle of attack is attributed to the lesser interaction of the shock wave oscillations with the leeward face of the frustum. With a larger angle of attack the conical bow shock wave reattaches very close to the frustum corner, allowing the separated shear layer to escape sooner, and as a consequence, providing a less severe pressure environment in the leeward side.

Table 1. Drag coefficients for the spike-nosed body

Angle of attack, deg.	C_D
0	1.1874
5	1.2846
10	1.3327

4. CONCLUSIONS

Supersonic flows at an angle of attack larger than zero over a spike-nosed body was numerically simulated. The flowfields for angles of attack of 5 and 10 degrees are characterized by a conical shock wave, a separated region in front of the body, and the interaction of the bow shock wave with reflected and reattachment shock waves. The separated region in front of the body is larger in the leeward side and the pressure environment is more severe in the windward side. The asymmetric shock wave structure is evident. Nevertheless, the principal mode of oscillation remains unaltered in both sides. The higher mode of oscillations in the leeward side are shift or not present when compared with the mode of oscillations in windward side or the axisymmetric flow.

Integrated forces showed large amplitudes of oscillations in the axial and normal directions. In the lateral direction small amplitude oscillations were observed due to the break down of vortices induced by the cross flow on the sides of the spike surface. The drag coefficient increased with increasing angle of attack. However the rate of increase reduced as the angle of attack increased.

A good agreement is obtained between the present computation and the available experimental data for the axisymmetric flow.

5. ACKNOWLEDGMENTS

The Centro Nacional de Supercomputação - UFRGS provided time on the Cray Y-MP computer. The author gratefully acknowledges this support.

6. REFERENCES

Crawford, D.H., Investigation of the Flow Over a Spike-Nose Hemisphere-Cylinder at Mach Number of 6.8, *NASA TN D-118*, Dec. 1959.

Bogdonoff, S.M., and Vas, I.E., Preliminary Investigations of Spiked Bodies at Hypersonic Speeds, *Journal of the Aero/Space Sciences*, Vol. 26, N. 2, Feb. 1959, pp.65-74.

Demetriades, A., and Hopkins, A.T., Asymmetric Shock-Wave Oscillations on Spiked Bodies of Revolution, *Journal of Spacecraft*, Vol. 13, N. 11, Nov. 1976, pp. 703-704.

Calarese, W., and Hankey, W.L. Modes of Shock-Wave Oscillations on Spike Tipped Bodies, *AIAA Journal*, vol. 23, N. 2, Feb. 1985, pp.185-192.

Shang, J.S., Hankey, W.L., and Smith, R.E., Flow Oscillations of Spike-Tipped Bodies, *AIAA Paper 80-0062*, Jan. 1980.

Shoemaker, J.M., Aerodynamic Spike Flowfields Computed to Select Optimum Configuration at Mach 2.5 With Experimental Validation, *AIAA paper 90-0414*, Jan. 1990.

Mikhail, A.G. Spike-Nosed Projectiles: Computations and Dual Flow Modes in Supersonic Flight, *Journal of Spacecraft*, vol. 28, N. 4, pp. 418-424, July-Aug. 1991.

Mikhail, A.G. Spike-Nosed Projectiles With Vortex Rings: Steady and Nonsteady Flow Simulations, *Journal of Spacecraft and Rockets*, vol. 33, n. 1, pp. 8-14, Jan.-Feb. 1996.

Yoon, S. and Kwak, D., Implicit Navier-Stokes Solver For Three-Dimensional Compressible Flow, *AIAA Journal*, vol. 30, pp. 2653-2659, November 1992.

Matsuno, K., A Time-Accurate Iterative Scheme For Solving the Unsteady Compressible Flow Equations, *AIAA Paper 89*-1992CP, 1989.

Morgenstern, A. Jr., Supersonic Flow Over a Spike-Nosed Body of Revolution, *Proceedings of the XIV COBEM*, paper code 236, theme nº 32, 1997.